2016

Effects Of Magnetic Drift Shell Splitting On Electron Diffusion In The Radiation Belts

Liheng Zheng

A. A. Chan

T. P. O'Brien

W. Tu

G. S. Cunningham

See next page for additional authors

AGU PUBLICATIONS

JGR

Journal of Geophysical Research: Space Physics

RESEARCH ARTICLE
10.1002/2016JA023438

Key Points:
- Magnetic drift shell splitting in geomagnetic field moves radiation belt electron sources to smaller L shells
- With typical electron phase space density profiles, drift shell splitting reduces radiation belt electron enhancement
- The reduction of electron enhancement has a limit corresponding to 2-D local diffusion on a curved surface in phase space

Correspondence to:
L. Zheng,
zhengliheng@gmail.com

Citation:
Zheng, L., A. A. Chan, T. P. O'Brien, W. Tu, G. S. Cunningham, J. M. Albert, and S. R. Elkington (2016), Effects of magnetic drift shell splitting on electron diffusion in the radiation belts, *J. Geophys. Res. Space Physics*, *121*, 11,985–12,000, doi:10.1002/2016JA023438.

Received 8 SEP 2016
Accepted 29 NOV 2016
Accepted article online 7 DEC 2016
Published online 28 DEC 2016

Effects of magnetic drift shell splitting on electron diffusion in the radiation belts

Liheng Zheng[1,2], A. A. Chan[1], T. P. O'Brien[3], W. Tu[4], G. S. Cunningham[5], J. M. Albert[6], and S. R. Elkington[7]

[1]Department of Physics and Astronomy, Rice University, Houston, Texas, USA, [2]Now at William B. Hanson Center for Space Sciences, University of Texas at Dallas, Richardson, Texas, USA, [3]Space Sciences Department, The Aerospace Corporation, El Segundo, California, USA, [4]Department of Physics and Astronomy, West Virginia University, Morgantown, West Virginia, USA, [5]Space Science and Applications Group, Los Alamos National Laboratory, Los Alamos, New Mexico, USA, [6]Air Force Research Laboratory, Space Vehicles Directorate, Kirtland Air Force Base, New Mexico, USA, [7]Laboratory for Atmospheric and Space Physics, University of Colorado Boulder, Boulder, Colorado, USA

Abstract Drift shell splitting in the presence of pitch angle scattering breaks all three adiabatic invariants of radiation belt electron motion and produces new diffusion terms that fully populate the diffusion tensor in the Fokker-Planck equation. The Radbelt Electron Model (REM) solves such a Fokker-Planck equation and is used to investigate the phase space density sources. Our simulation results and theoretical arguments suggest that drift shell splitting changes the phase space location of the source to smaller L shells, which typically reduces outer zone phase space density enhancements, and this reduction has a limit corresponding to two-dimensional local diffusion on a curved surface in the phase space.

1. Introduction

Radiation belt dynamics can be simulated by solving a Fokker-Planck equation in a set of phase space coordinates with a given diffusion tensor [e.g., *Schulz and Lanzerotti*, 1974]. In an axially symmetric magnetic field, such as a dipole field, particle drift shells do not depend on equatorial pitch angle α_0, which is then a constant along a drift trajectory, and the variables α_0, mechanical momentum p, and Roederer's L [*Roederer*, 1970, section III.2] are useful phase space coordinates. When axial symmetry is broken, as in the geomagnetic field, α_0 is no longer constant for the entire drift shell. This necessitates the use of adiabatic invariants J_1, J_2, and J_3, or equivalently and more conventionally M, K, and L, as coordinates of the phase space. As defined in *Schulz* [1996], M is equal to the product of the electron's magnetic moment with its Lorentz factor γ, K is a field geometric quantity depending on the electron's mirror points but not energy, and L is inversely proportional to the amount of magnetic flux enclosed by the electron's drift shell. Moreover, in an asymmetric magnetic field L becomes dependent on α_0, i.e., drift shells would split for an ensemble of originally colocated particles with different α_0 [e.g., *Roederer*, 1967], which gives rise to the terminology "drift shell splitting." For relativistic electrons in the outer radiation belt, magnetic field asymmetry is the dominant mechanism of drift shell splitting [*Schulz and Lanzerotti*, 1974, section III.7], and this study is restricted to it.

The dependence of L on α_0 introduces new components to the diffusion tensor. This occurs as one transforms the two-dimensional (2-D) bounce-averaged diffusion tensor from the (α_0, p, L) coordinates to the (M, K, L) coordinates on a guiding field line:

$$\begin{pmatrix} D_{MM} & D_{MK} & D^*_{ML} \\ D_{MK} & D_{KK} & D^*_{KL} \\ D^*_{ML} & D^*_{KL} & D^*_{LL} \end{pmatrix} = \begin{pmatrix} \frac{\partial M}{\partial \alpha_0} & \frac{\partial M}{\partial p} & 0 \\ \frac{\partial K}{\partial \alpha_0} & 0 & 0 \\ \frac{\partial L}{\partial \alpha_0} & 0 & 1 \end{pmatrix} \begin{pmatrix} \mathcal{D}_{\alpha_0\alpha_0} & \mathcal{D}_{\alpha_0 p} & 0 \\ \mathcal{D}_{\alpha_0 p} & \mathcal{D}_{pp} & 0 \\ 0 & 0 & 0 \end{pmatrix} \begin{pmatrix} \frac{\partial M}{\partial \alpha_0} & \frac{\partial K}{\partial \alpha_0} & \frac{\partial L}{\partial \alpha_0} \\ \frac{\partial M}{\partial p} & 0 & 0 \\ 0 & 0 & 1 \end{pmatrix}. \quad (1)$$

Here the starred components are generated by drift shell splitting. In addition to the M-L and K-L off-diagonal components, a new "unconventional" radial diffusion component, conserving M and K, arises due to pitch angle scattering and drift shell splitting. With vanishing $\partial L/\partial \alpha_0$ in the Jacobian matrix, D^*_{ML}, D^*_{KL}, and D^*_{LL} also vanish, leaving the left-hand side tensor still a 2×2 block.

Based on the above transformation, *O'Brien* [2014, 2015] calculated the bounce-and-drift-averaged chorus wave diffusion tensor using a statistical chorus wave model (as in *Shprits et al.* [2011]), the *Sheeley et al.* [2001] plasma density model, and realistic geomagnetic field models. These geomagnetic field models include the International Geomagnetic Reference Field [*Finlay et al.*, 2010], which provides effects of the Earth's internal magnetic multipoles, and the T89 model [*Tsyganenko*, 1989], which provides the external magnetic field asymmetry. In those calculations, field-aligned chorus wave propagation was assumed, as an approximation to the full distribution of propagation angles. *Shprits and Ni* [2009] showed that the field-aligned calculation grossly matches the much more expensive calculation accounting for oblique waves, and *Santolík et al.* [2010] showed that chorus waves observed in the outer zone are often nearly field aligned. Only chorus waves were considered because of our focus on the outer zone where drift shell splitting is most significant. Hiss and electromagnetic ion cyclotron waves can be present in the outer zone in a plasmaspheric plume, but no plume is assumed in this study. Observational evidence points strongly to a dominant role for chorus in outer zone dynamics [e.g., *Liu et al.*, 2015], and chorus is typically the only wave mode accounted for outside the plasmasphere in simulations [e.g., *Tu et al.*, 2014]. *O'Brien* [2015] included a discussion of the potential shortcomings of these assumptions, but we accept them as published for this study. From *O'Brien* [2015], the drift-averaged magnitudes of the starred diffusion components in (1) are comparable to or even larger than the unstarred counterparts for low-energy electrons (~100 keV) in the midnight α_0 range 40° to 80°, suggesting possible strong effects on the "seed" population. As energy increases into the MeV range, the starred components become insignificant. This paper investigates the effect of drift shell splitting on radiation belt electron diffusion using the diffusion tensor calculated by *O'Brien* [2015].

2. Simulation of an Idealized MeV Electron Enhancement

2.1. Simulation Setup

We use REM to numerically investigate drift shell splitting effects on the electron phase space density (PSD). REM is a gridless 3-D electron diffusion model that works in adiabatic invariant coordinates. Based on the stochastic differential equation method [e.g., *Tao et al.*, 2008; *Zheng et al.*, 2014], REM can solve the Fokker-Planck equation with a fully populated 3-D diffusion tensor in a complex shaped domain. Good statistics of the solution are guaranteed by the adaptive methods used in REM [*Zheng*, 2015]. In this study, the simulation domain is defined in adiabatic invariant space by electron kinetic energy E from 100 keV to 10 MeV, K from the bounce loss cone to zero or the drift loss cone, and L from 2 to 8. The mapping between E and adiabatic invariants is attained by the relation

$$E = \mathcal{E}_0 \left(\sqrt{\frac{2B_m M}{\mathcal{E}_0} + 1} - 1 \right), \tag{2}$$

where $\mathcal{E}_0$ (= 0.511 MeV) is electron rest energy and the mirror point magnetic intensity B_m is tabulated as a function of K and L via particle tracing in the geomagnetic field model.

To examine drift shell splitting effects on electron PSD, we have made simulations of a model storm motivated by the 8 October 2012 electron acceleration event, during which the 100 keV electron flux was observed to increase exponentially for about 7 h and to stay steady afterward [*Tu et al.*, 2014]. The injection onset is the starting point of our simulations. We emphasize that our purpose is not to precisely reproduce this specific event but to evaluate the magnitude of the drift shell splitting effect on the electron PSD using a representative idealized simulation that can be easily understood.

Early theoretical studies had assessed drift shell splitting effects assuming that the electron PSD profile had a positive L gradient at constant M and K and a negative L gradient at constant E and α_0 beyond a peak [*Schulz and Lanzerotti*, 1974, p. 107, and references therein]. Though not always a realistic assumption, recent observations [e.g., *Onsager et al.*, 2004; *Kim et al.*, 2010; *Boyd et al.*, 2014], however, showed that the typical hundred keV electron PSD profile is indeed more often than not in this case. To be comparable with historical studies, we design our simulation initial and boundary conditions to both keep this historical assumption and feature event-specific observations. These initial and boundary conditions are obtained from 3-D time-dependent fit to Van Allen Probes electron flux observations at $L = 4$ during the 8 October 2012 storm, using approximate analytic solutions of a simplified Fokker-Planck equation as fitting functions (see Appendix A for details). We note that neither energy diffusion nor drift shell splitting exists in this initial condition; rather, they develop as the simulation begins. Dirichlet boundary conditions share the same functional form as the initial condition,

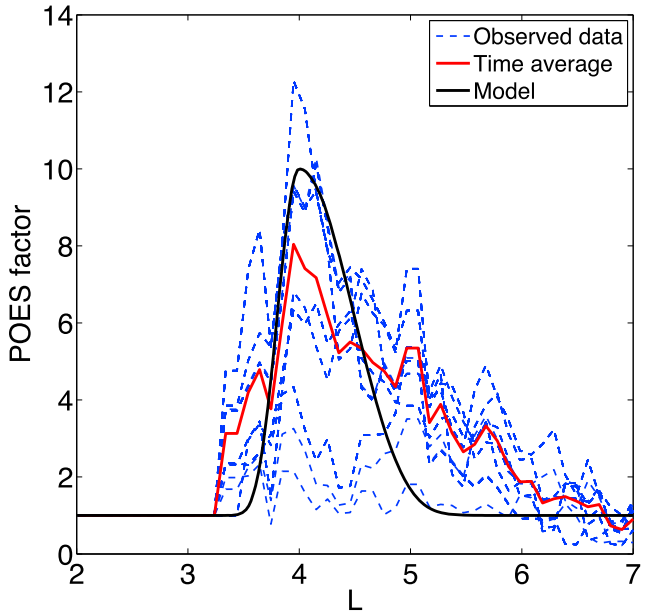

Figure 1. Real-time magnetic local time (MLT)-averaged POES factors for every half hour from 23:00 UT 8 October 2012 to 16:00 UT 9 October 2012 (blue dashed lines), their time average during this period (red solid line), and the model POES factor with a peak height of 10 at $L = 4$ (black solid line). Model POES factors of a different peak height (namely 4, 7, and 13) have the same peak location and width as the one shown here.

except that they contain data-fitted time-dependent factors that characterize the seed electron flux injection, which also guarantee consistency between initial and boundary conditions.

In contrast to a simulation in a dipole field, in an asymmetric geomagnetic field a new phase space boundary arises due to electron Shabansky orbits [*Shabansky*, 1971; *Öztürk and Wolf*, 2007], on which the electron drift trajectories bifurcate into either of the two magnetic field minima before local noon and join together afterward. The Roederer L for electrons on these orbits is not defined [*Ukhorskiy et al.*, 2011], so that the electrons are not describable by and must be excluded from the 3-D adiabatic invariant phase space. Further, these electrons are quasi-trapped; they drift from a few to a few hundred periods depending on the orbit before escaping into the bounce or drift loss cone [*Ukhorskiy et al.*, 2011]. Therefore, in addition to a PSD source as electrons are fed in the nightside from the quasi-trapped region to the stably trapped region, this boundary also serves as a loss of radiation belt electrons. A 50 drift period exponential decay is imposed to its Dirichlet boundary condition to primitively reflect these mechanisms (see Appendix A). Phase space locations of this boundary are determined from particle tracing in the geomagnetic field model.

This study adopts *Ozeke et al.* [2014] ULF wave diffusion coefficients (D_{LL}^{ULF}) to invoke the conventional radial diffusion at constant M and K, and the aforementioned *O'Brien* [2015] drift shell splitting chorus wave diffusion coefficients (the drift average of D_{ij} in the left-hand side of equation 1), so that the Fokker-Planck equation solved is

$$\frac{\partial \bar{f}}{\partial t} = \frac{1}{G}\frac{\partial}{\partial Q_i}\left(G\langle D_{ij}\rangle \frac{\partial \bar{f}}{\partial Q_j}\right) + L^2\frac{\partial}{\partial L}\left(\frac{1}{L^2}D_{LL}^{\mathrm{ULF}}\frac{\partial \bar{f}}{\partial L}\right), \tag{3}$$

where $\bar{f}$ is the phase-averaged PSD, G is the Jacobian determinant for the coordinate transform from (J_1, J_2, J_3) to (M, K, L) as represented collectively by the Q_is, and summation over repeated indices is implied. The *Ozeke et al.* [2014] radial diffusion coefficients are derived from statistical representations of compressional magnetic field wave power and azimuthal electric field wave power in the ULF band and are analytically approximated as functions of L and Kp. As a simple but reasonable storm time value, we assume constant $Kp = 4$, which also results in significant asymmetry in the T89 magnetic field [*O'Brien*, 2015]. To better resemble the 8 October 2012 storm, we multiply the statistically obtained chorus wave amplitudes by event-specific factors inferred from POES spacecraft data [e.g., *Li et al.*, 2013; *Chen et al.*, 2014], so that the *O'Brien* [2015] diffusion coefficients

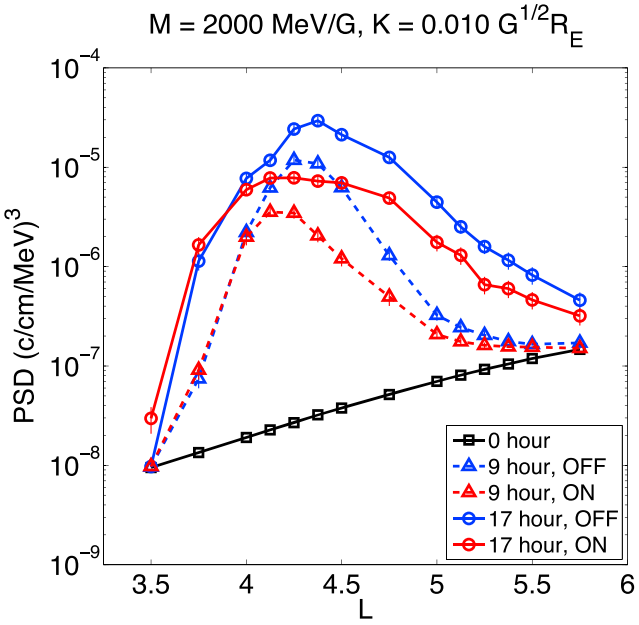

Figure 2. REM-simulated PSD radial profiles with drift shell splitting off (blue) and on (red) for $M = 2000$ MeV/G and $K = 0.01\,\mathrm{G}^{\frac{1}{2}} R_E$ at $t = 9$ h (dashed) and $t = 17$ h (solid). The vertical bar at each data point indicates the estimated 90% confidence interval of the solution.

are multiplied by the POES factors squared. In our simulation, these POES factors have a radial profile that peaks at $L = 4$ with a height of 10 as shown in Figure 1.

2.2. Simulation Results

Figure 2 plots the radial profile of PSD solutions at $M = 2000$ MeV/G and $K = 0.01\,\mathrm{G}^{\frac{1}{2}} R_E$ at 9 and 17 h after the initial time, with comparisons in which effect of drift shell splitting is turned on or off by retaining or removing the starred components in equation (1). In both cases, strong local acceleration produces PSD peaks in the heart of the radiation belt. Inside $L = 4$, the "on" and "off" solutions are very close because of small asymmetry in the inner geomagnetic field. Beyond $L = 4$, the on solutions are all lower than the off solutions, with the largest discrepancy appearing around the PSD peaks.

To better investigate the diffusion processes, we use REM to generate PSD source plots for a given phase space solution point. These plots show the PSD contribution from various phase space locations to that solution point. Figure 3 shows source plots for the off (Figures 3a–3c) and on (Figures 3d–3f) solutions at the PSD peaks ($L = 4.4$, $t = 17$ h) in Figure 2. From left to right in each row, the three panels are projections of the 3-D PSD source distribution along E, α_0, and L dimensions, respectively. Each pixel in these panels represents a 2-D phase space element, whose color represents the amount of PSD it contributes to the solution point (indicated by the cross). In these plots and sections 2 and 3, the definition of α_0 on a drift shell is generalized using the mirror point magnetic intensity $B_m(K)$, which is a drift invariant, compared to that of the equatorially bouncing electrons with the same L:

$$\sin^2 \alpha_0(K)\Big|_L \equiv \frac{B_m(0)}{B_m(K)}\Big|_L . \tag{4}$$

This generalized α_0 is hence also drift invariant and reduces to equatorial pitch angle if the field is reduced adiabatically to a symmetric field, where the two drift shells employed in this definition degenerate.

A striking feature of Figure 3 is that in both off and on solutions, the majority of the PSD comes from a narrow range of L around 4.4 near the low-energy boundary, suggesting that local acceleration together with the seed population plays a decisive role in electron energization, and the diffusion is approximately 2-D α_0-E diffusion. The seed electron source region in the on case (Figures 3d and 3e) is broader in L than in the off case (Figures 3a and 3b). The low-energy sources in the off case (Figure 3b) occur roughly at $L = 4.4$, whereas in the on case (Figure 3e) they occur at a lower L around 4.2. The α_0 distribution of the sources in both cases

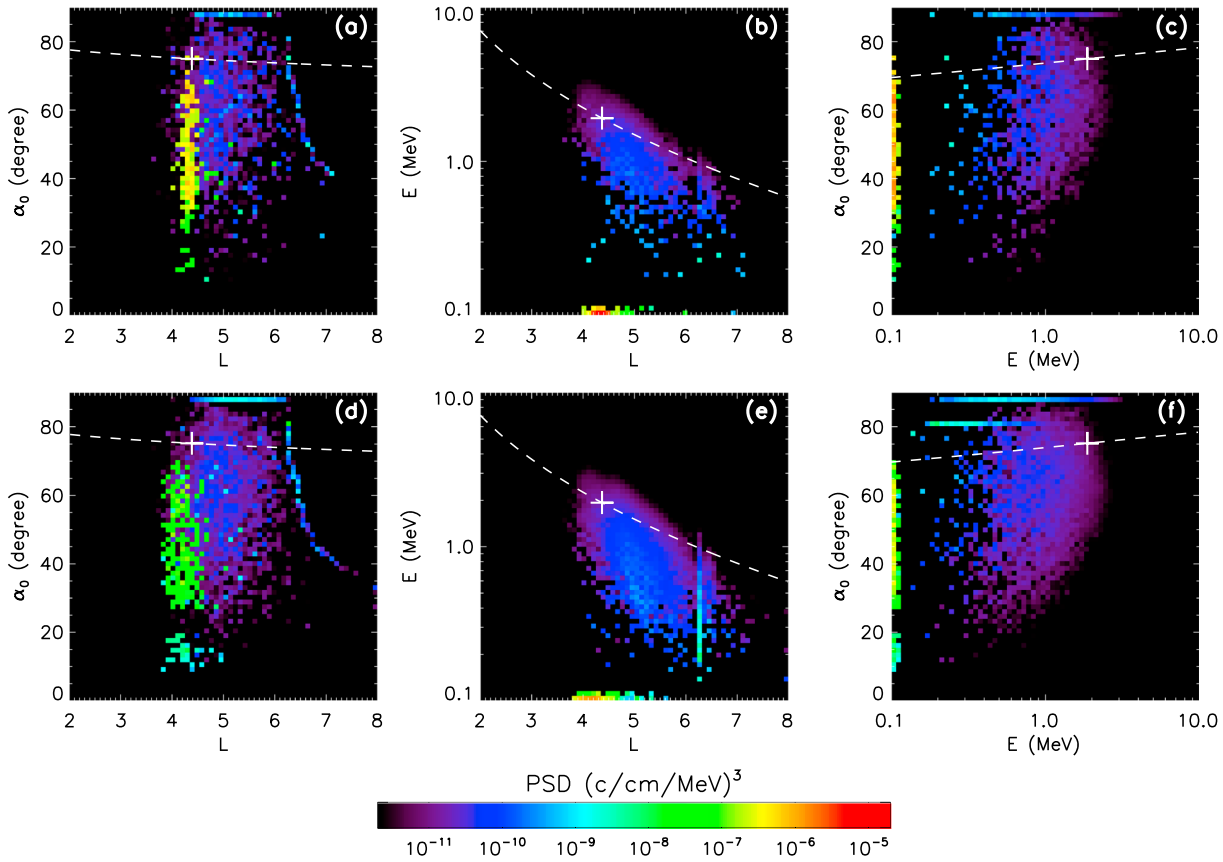

Figure 3. PSD source plots for the $t = 17$ h solutions at $M = 2000$ MeV/G, $K = 0.01\,\mathrm{G}^{\frac{1}{2}} R_E$, and $L = 4.4$ (white cross), with drift shell splitting (a–c) off and (d–f) on. White dashed lines are projections of the 3-D constant M and K curve, or "radial diffusion curve" through the cross, calculated with dipole field geometry. The lines of dark blue pixels within $L = 6$–8 and $\alpha_0 = 40°$–$90°$ in Figures 3a and 3d indicate locations of the Shabansky orbit boundary.

(Figures 3a and 3d) has two blobs, one between 25° and 70° corresponding to energization from the nightside chorus and the other below 20° from the dayside chorus.

The prominence of the drift shell splitting effect depends on the relative importance of chorus wave diffusion. The latter is a function of the peak height of the POES factors. In the large POES factor limit chorus wave scattering dominates, so that the diffusion is asymptotically 2-D, and in the opposite limit the diffusion approaches 1-D radial diffusion as illustrated in Figure 4, and the drift shell splitting effect vanishes. Figure 5 plots the difference of PSD solutions (off minus on) at $L = 4.4$ and $t = 17$ h versus a range of peak POES factors. Regardless of the POES factor value, all the PSD differences are positive. As the POES factor increases, the PSD difference increases monotonically but approaches a 2-D diffusion limit as approximated by the dashed line, which is the difference calculated using peak POES factor 13 but without ULF wave diffusion. (The ro points are referred to in section 4.) The ratio of PSD solutions (off over on) is shown in Figure 6. Comparing Figure 5 with Figure 6 shows that the difference of PSD has a simpler and more meaningful dependence on POES factors than the ratio of PSD. In the next section, we use analytic theory to investigate the changes in PSD due to drift shell splitting and to interpret these simulation results.

3. Theoretical Analysis

Let us start with the bounce-averaged diffusion on a guiding field line. Symbolically, equation (1) can be written as $\boldsymbol{D} = \boldsymbol{G}\mathcal{D}\boldsymbol{G}^{\mathrm{T}}$, where different fonts of the diffusion tensors denote their different coordinates. By construction, the diffusion tensor $\mathcal{D}$ has two positive (or zero) eigenvalues, whose corresponding eigenvectors are the semiaxes of the elliptic contour of the diffusion Green function [cf. *Albert*, 2009] in the α_0-p plane,

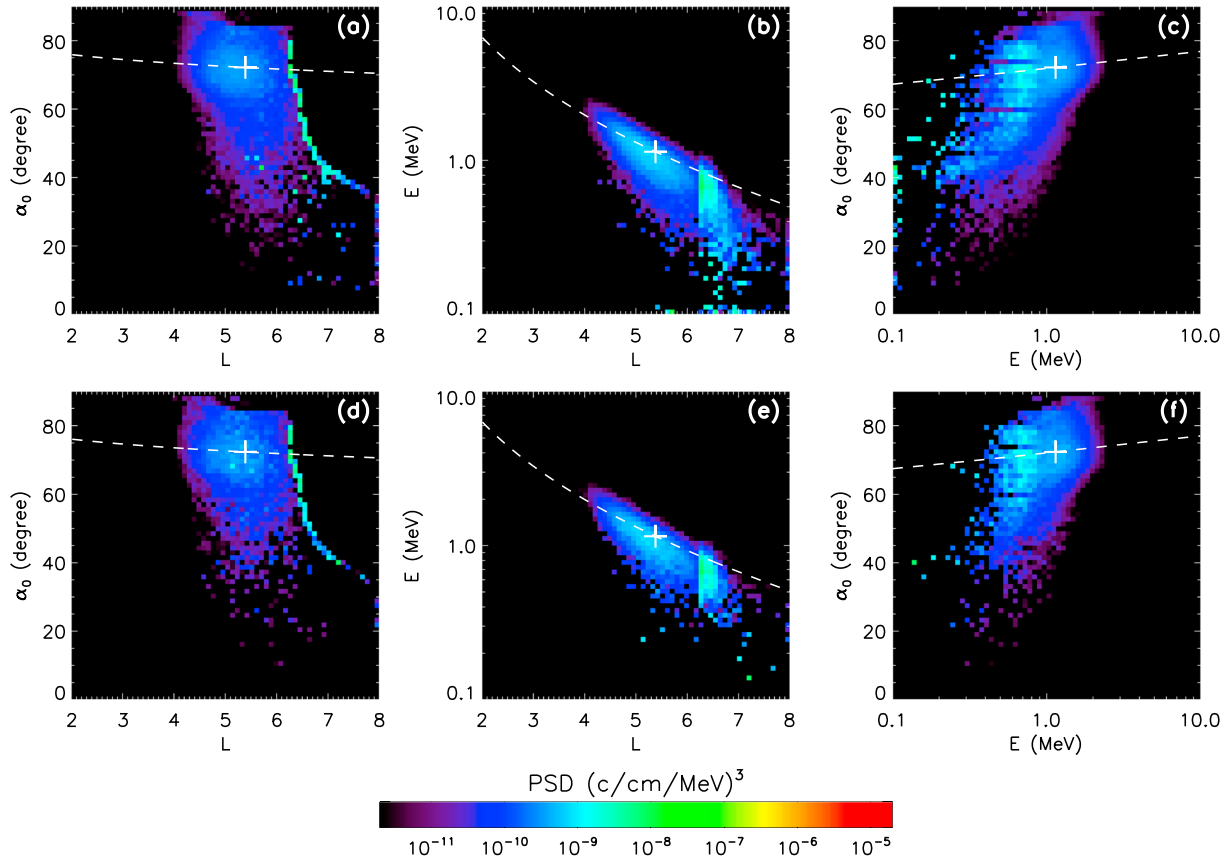

Figure 4. PSD source plots, in the same format as Figure 3, for the $t = 17$ h solutions at $M = 2000$ MeV/G, $K = 0.01\,G^{\frac{1}{2}}R_E$, and $L = 5.4$, calculated with uniform POES factor 1. (a and d) The Shabansky orbit boundary is seen as the line of green pixels. (b and e) The energization mechanism here is primarily radial diffusion, with the majority of PSD contributed by the Shabansky orbit boundary.

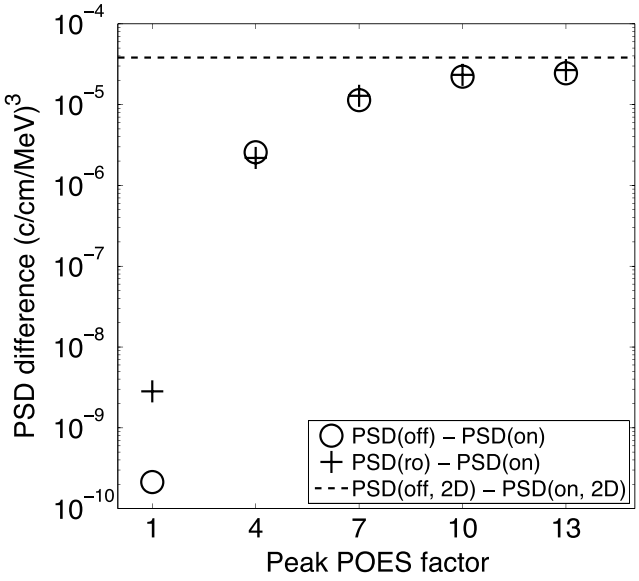

Figure 5. Difference in PSD solutions at $M = 2000$ MeV/G, $K = 0.01\,G^{\frac{1}{2}}R_E$, $L = 4.4$, and $t = 17$ h versus the peak height of the POES factor. In the legend, off or on indicates that drift shell splitting is turned off or on, "ro" means only $\langle D^*_{LL}\rangle$ is included and not $\langle D^*_{ML}\rangle$ or $\langle D^*_{KL}\rangle$, and "2D" means the simulation is done with a peak POES factor 13 and no ULF wave diffusion. At "peak" POES factor 1, the POES factor is actually uniformly 1 with no peak.

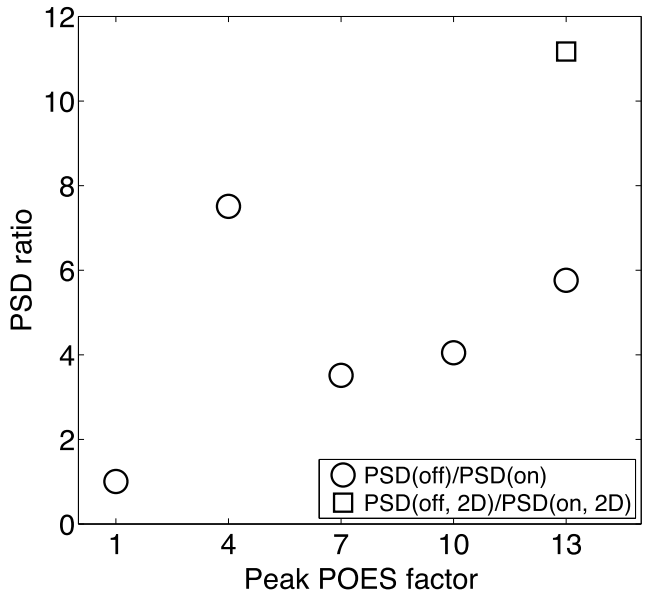

Figure 6. Ratio between PSD solutions at the same phase space location and time as in Figure 5. At POES factor 1, the PSD ratio is very close to 1, indicating that the drift shell splitting effect is very weak. As the peak POES factor increases, both local acceleration and the drift shell splitting effect increase, and their competition results in a nonmonotonic relation between the PSD ratio and the strength of chorus wave diffusion. At a moderate peak POES factor 4, the ratio reaches a local maximum where on is nearly 1 order of magnitude smaller than off.

and a third trivially zero eigenvalue with the eigenvector in the L direction. Arranging eigenvalues in descending order, this corresponds to a diagonalized factorization of $\boldsymbol{\mathcal{D}}$ such that

$$\boldsymbol{\mathcal{D}} = \left(\hat{\boldsymbol{u}} \ \hat{\boldsymbol{v}} \ \hat{\boldsymbol{l}} \right) \begin{pmatrix} \lambda_1 & & \\ & \lambda_2 & \\ & & 0 \end{pmatrix} \begin{pmatrix} \hat{\boldsymbol{u}}^{\mathsf{T}} \\ \hat{\boldsymbol{v}}^{\mathsf{T}} \\ \hat{\boldsymbol{l}}^{\mathsf{T}} \end{pmatrix}, \quad (\lambda_1 \geq \lambda_2 \geq 0), \tag{5}$$

in which $\hat{\boldsymbol{u}}$ and $\hat{\boldsymbol{v}}$ are orthogonal unit eigenvectors corresponding to eigenvalues λ_1 and λ_2 and $\hat{\boldsymbol{l}}$ is the unit vector along the L axis. In mathematics, the continuous one-to-one mapping of a coordinate transform conserves topology of a geometrical object (homeomorphism [cf. *Zorich*, 2004]). Therefore, although the (M, K, L) space is not metric, we are still able to discuss topology of a geometrical object within, for it is identical to that in the (J_1, J_2, J_3) space, whereas the latter space is physically a Euclidean space of the generalized momenta. For the topological discussion in this section, we understand the coordinate variables as dimensionless as being scaled by proper dimensional constants.

According to Sylvester's law of inertia [e.g., *Norman*, 1986, pp. 360–361], the congruence transform in (1) conserves the numbers of positive and zero eigenvalues of the diffusion tensors on both sides. Therefore, although fully populated, the left-hand side tensor $\boldsymbol{D}$ is nonetheless singular due to the zero eigenvalue. At a given point in the (M, K, L) space, the bounce-averaged diffusion is hence in a local 2-D plane containing the first two eigenvectors of $\boldsymbol{D}$. In general, it is difficult to analytically calculate these eigenvectors to obtain the orientation of the plane. However, since the plane is just the local α_0-p plane after a coordinate transform, the transformed $\hat{\boldsymbol{u}}$ and $\hat{\boldsymbol{v}}$ vectors, denoted as $\boldsymbol{\xi}$ and $\boldsymbol{\eta}$, respectively, must also lie in this plane, where $\boldsymbol{\xi}$ and $\boldsymbol{\eta}$ are readily given by the matrix equation

$$\left(\boldsymbol{\xi} \ \boldsymbol{\eta} \right) = \mathbf{G} \left(\hat{\boldsymbol{u}} \ \hat{\boldsymbol{v}} \right). \tag{6}$$

Thus, the normal of the local 2-D diffusion plane points in the direction of

$$\boldsymbol{n} = \boldsymbol{\xi} \times \boldsymbol{\eta} = \frac{\partial M}{\partial p} \left(\frac{\partial L}{\partial \alpha_0} \hat{\boldsymbol{k}} - \frac{\partial K}{\partial \alpha_0} \hat{\boldsymbol{l}} \right), \tag{7}$$

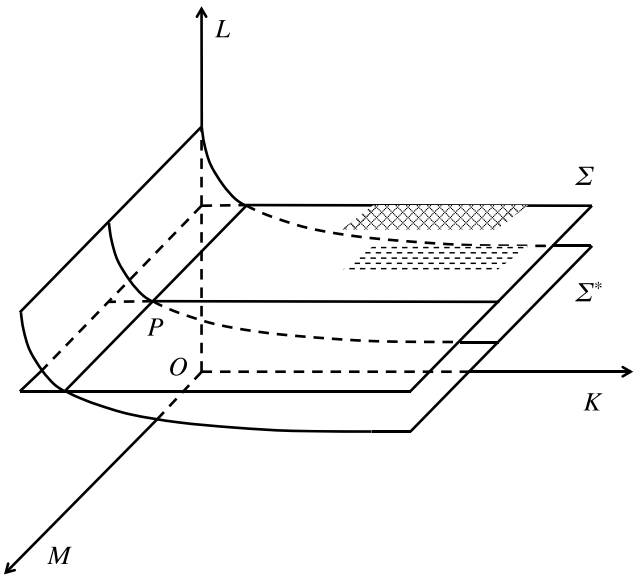

Figure 7. Schematic illustration of a bounce-averaged diffusion surface for a nightside guiding field line in a symmetric magnetic field (the Σ plane), and in an asymmetric geomagnetic field (the Σ^* surface), with a common L value at the phase space point P. The intersection of Σ and Σ^* through P is a straight line parallel with the M axis. Shaded areas indicate the phase space regions of the seed electrons (see text). The Σ^* surface for a dayside guiding field line would be tilted upward in L with increasing K, due to negative $\partial L/\partial\alpha_0$.

where $\hat{\boldsymbol{k}}$ is the unit vector along the K axis. This is also the direction of the third eigenvector of $\boldsymbol{D}$, corresponding to its zero eigenvalue.

In equation (7), $\partial M/\partial p\ (=2M/p)$ is positive, and $\partial L/\partial\alpha_0$ and $\partial K/\partial\alpha_0$ are field geometric quantities, with $\partial K/\partial\alpha_0$ always negative except at $\alpha_0 = \pi/2$ where it vanishes. Thus, the direction of $\boldsymbol{n}$ is solely determined by the geometry of the guiding field line. For a symmetric field, because $\partial L/\partial\alpha_0$ is identically zero, $\boldsymbol{n}$ is uniformly in the $\hat{\boldsymbol{I}}$ direction and the diffusion is confined in an M-K plane. For the asymmetric geomagnetic field, $\boldsymbol{n}$ tilts in the $\hat{\boldsymbol{k}}$ direction by an amount that depends on the sign and relative magnitude of $\partial L/\partial\alpha_0$ compared to $\partial K/\partial\alpha_0$. In particular, $\partial L/\partial\alpha_0$ is typically positive for guiding field lines in the nightside and negative for those in the dayside [cf. *O'Brien*, 2015, Figure 1; *Schulz and Lanzerotti*, 1974, section III.7], and $\partial K/\partial\alpha_0$ decreases without bound with decreasing α_0 (in dipole field, $\partial K/\partial\alpha_0 \sim -\cos\alpha_0/\sin^2\alpha_0$). At small K, the $\hat{\boldsymbol{k}}$ component of $\boldsymbol{n}$ dominates because of vanishing $\partial K/\partial\alpha_0$ as K approaches 0, but as K increases, since $\partial L/\partial\alpha_0$ cannot be boundless, the $\hat{\boldsymbol{I}}$ component quickly becomes significant and eventually dominates. For all M and K values on the guiding field line, all of these local planes thus form a curved surface in phase space, with its normal direction at every point given by $\boldsymbol{n}$. Figure 7 schematically illustrates such a surface for a guiding field line in the nightside. On this guiding field line, the 2-D bounce-averaged diffusion takes place in this surface (Σ^*) rather than in an M-K plane (Σ) as in a symmetric field. For a representative point stochastically scattering in Σ^*, its L value thus changes due to the geometry of the surface.

Different guiding field lines have different Σ^* diffusion surfaces, so a fixed phase space point, such as point P in Figure 7, resides on a family of Σ^* surfaces corresponding to all the guiding field lines on the drift shell, and these Σ^* surfaces all have the common straight-line intersection at constant K and L, since the drift shell is specified by these two parameters. At this point, though bounce-averaged diffusion on each guiding field line is confined to its individual surface, drift-averaged diffusion, as a superposition of the former, effectively takes place in a phase space volume. This means that the diffusion tensor loses its singularity after drift averaging [*O'Brien*, 2015]. In this sense, strict 2-D drift-averaged diffusion does not occur in an asymmetric geomagnetic field even without drift-resonant radial diffusion.

Because wave activity is not evenly distributed in magnetic local time, the bounce-averaged diffusion in each Σ^* surface contributes differently to the drift average. Outside the plasmapause, the diffusion rate

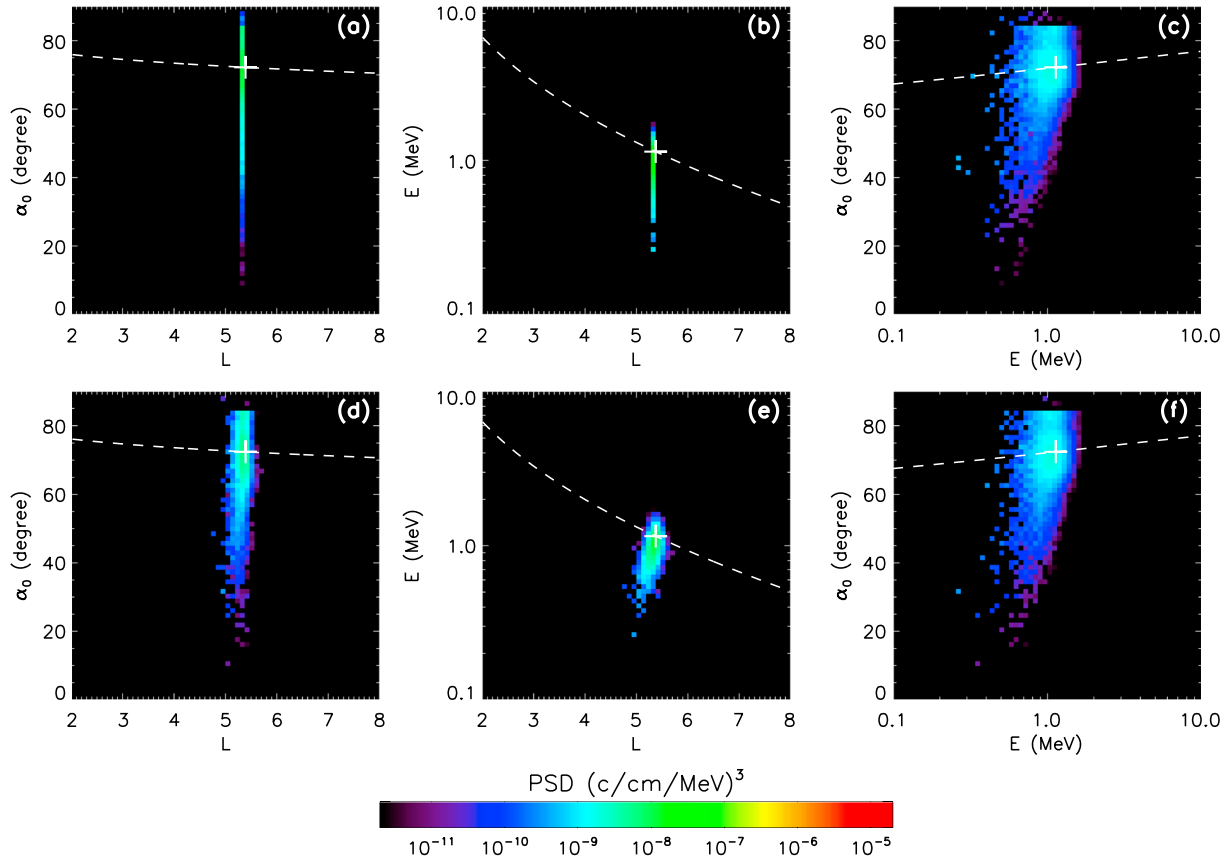

Figure 8. PSD source plots, in the same format as Figure 3, for the $t = 17$ h solutions at $M = 2000$ MeV/G, $K = 0.01\,G^{\frac{1}{2}}R_E$ and $L = 5.4$, calculated with the 2-D diffusion setup (see text). In the off case (a–c), PSD sources are distributed in the $L = 5.4$ plane. In the on case (d–f), PSD sources are distributed near a surface that tilts toward smaller L at smaller α_0s and smaller Es than the solution point (cross).

of nightside chorus typically exceeds that of dayside chorus by orders of magnitude except at small α_0s [e.g., *Li et al.*, 2007; *Thorne et al.*, 2010]. Consequently, except at large K, the drift-averaged diffusion would primarily take place along the Σ^* surfaces of nightside guiding field lines. At large K, the shapes of all Σ^* surfaces are close to an M-K plane anyway due to the dominant $\hat{\boldsymbol{I}}$ component in the normal and thus make little difference to the drift-averaged diffusion. As a result, the drift-averaged chorus wave diffusion in an asymmetric geomagnetic field is still approximately 2-D, around a surface in the phase space similar to that of a nightside guiding field line.

This approximate 2-D drift-averaged diffusion is indeed observable in the PSD source plots. Figure 8 shows source plots for solutions at $M = 2000$ MeV/G, $K = 0.01\,G^{\frac{1}{2}}R_E$, $L = 5.4$, and $t = 17$ h from the simulations of Figure 5 that are labeled 2D. In the off case (Figures 8a–8c), PSD sources align exactly in the constant $L = 5.4$ plane, whereas in the on case (Figures 8d–8f), PSD sources are distributed near a surface that tilts toward smaller L in smaller α_0 and smaller E. This is consistent with the theoretically predicted 2-D diffusion near the Σ^* surface in Figure 7, where PSD sources contributing to the point P from smaller M and larger K regions have smaller L values than that of P, due to the geometry of the surface. The same phenomenon is also observed in the source plots for the solution with the same M, K, and t but at $L = 4.4$, as shown in Figure 9. In this case, the PSD sources are mainly from the low-energy boundary instead of the interior phase space. PSD contributions from the portion of the Σ^* surface that is at smaller K and larger L to the solution point are visible in Figures 8d and 8e.

On the basis of this discussion, we can now better understand the results in section 2. In Figure 3, the solution point is at smaller K than the range of strong chorus wave scattering, which occurs for generalized α_0 between

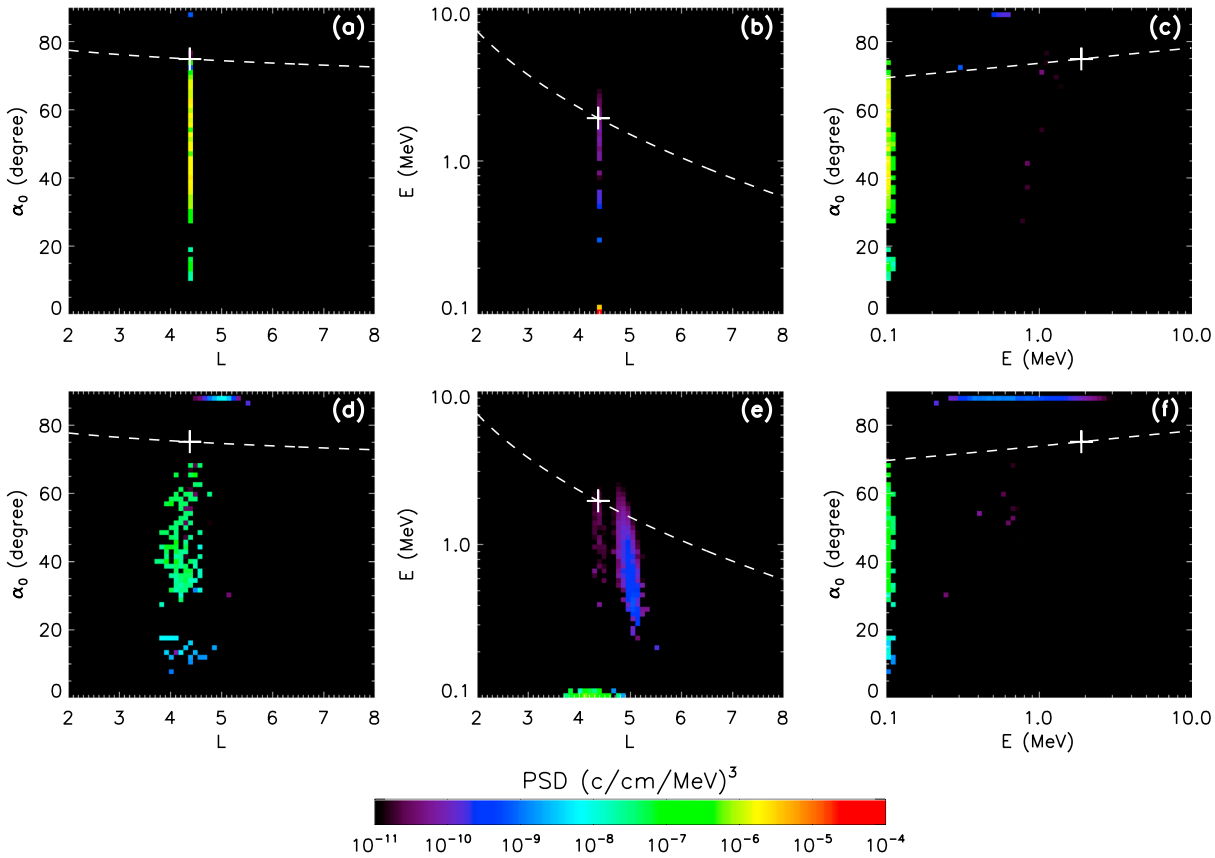

Figure 9. PSD source plots, in the same format as Figure 3, for the $t = 17$ h solutions at $M = 2000$MeV/G, $K = 0.01\ \mathrm{G}^{\frac{1}{2}} R_E$, and $L = 4.4$, calculated with the 2-D setup. In the (a–c) off case, PSD sources are distributed in the $L = 4.4$ plane, mainly near the low-energy boundary. In the (d–f) on case, PSD sources are distributed near a surface that at smaller α_0s has L value smaller than that of the solution point (cross) and at larger α_0s has L value larger than that of the cross, as predicted in the theoretical explanation. Integration of the source distribution in Figure 9e along the E dimension indicates that it is centered at $L = 4.1$.

about 10° to 70°. By the geometry of the surfaces in Figure 7, the seed electrons for point P are located at a smaller L in the Σ^* surface than those in the Σ plane (as indicated by the shaded areas); this is why the seed electrons in the on case are from smaller L than those in the off case. Furthermore, drift shell splitting makes the drift average of $\boldsymbol{D}$ nonsingular, so that the seed electron regions in the on case are more spread in L. The PSD of the seed electrons typically has a positive gradient in L at fixed M and K, so it follows that local acceleration of the seed electrons from smaller L provides less PSD. The lower PSD solutions with drift shell splitting in Figure 2 are consistent with this mechanism. One caveat is that a difference in chorus wave diffusion rates on Σ^* and Σ may also have an effect and that should be investigated in future work.

In Figure 7, as the point P moves toward larger K into the range of strong chorus wave scattering, the Σ^* surface is raised in L so that its intersection with the Σ plane goes through the shaded areas, and the shaded areas are closer in L. Moreover, the shape of Σ^* at large K is close to that of Σ. Therefore, the drift shell splitting effect becomes negligible at large K, as demonstrated in Figure 10.

In Figure 5, when chorus wave diffusion is decreased by the decreasing peak POES factor, the source regions in Figure 7 are moved closer to P along the Σ^* surface or the Σ plane, so that they are less separated in L. Moreover, drift-resonant radial diffusion, which is then relatively stronger, would move these source regions in L and further spread them. As a result, the source regions will increasingly overlap, and the drift shell splitting effect diminishes. Because both the chorus wave acceleration effect and the drift shell splitting effect depend on the POES factors, the PSD differences in Figure 5 reveal a simpler relation to POES factor than the PSD ratios in Figure 6; in the latter, this relation is complicated by the competition between the two effects.

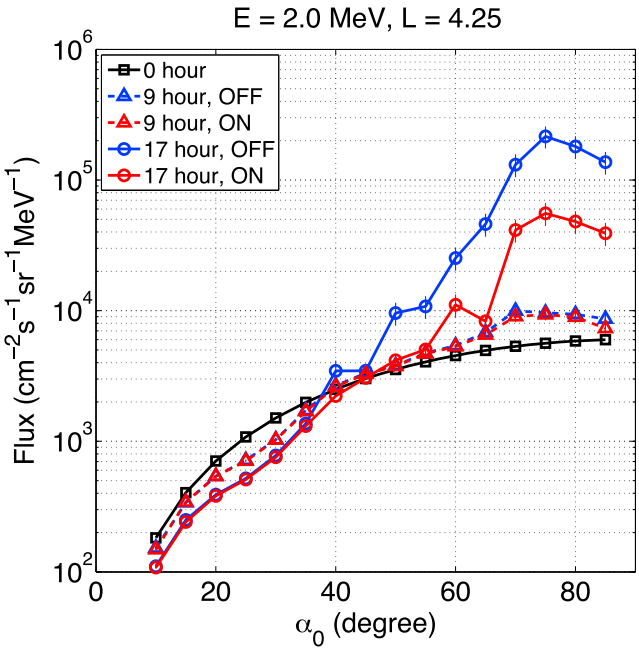

Figure 10. REM-simulated flux profiles in generalized α_0 with drift shell splitting off (blue) and on (red) for $E = 2.0$ MeV and $L = 4.25$ at $t = 9$ h (dashed) and $t = 17$ h (solid), calculated with a POES factor profile that peaks at $L = 5$ with a height 7. At $\alpha_0 \lesssim 40°$, the two 17 h solutions are effectively indistinguishable, suggesting that the drift shell splitting effect vanishes as K becomes large.

4. Discussion and Conclusions

Early drift shell splitting studies [e.g., *Fälthammar and Walt*, 1969; *Roederer and Schulz*, 1969; *Schulz*, 1972; *Schulz and Lanzerotti*, 1974, sections III.7 and III.8] focused mainly on anomalous radial diffusion caused by elastic pitch angle scattering in a distorted geomagnetic field. Since energy E is conserved in this process, the corresponding anomalous radial diffusion coefficient, as estimated by drift average of the L displacement at constant α_0 and E [e.g., *Schulz*, 1972], must be expressed in the (α_0, p, L) coordinates, and it is not the same as the $\langle D^*_{LL} \rangle$ obtained from a drift average of the left-hand side of equation (1). In these early studies, the drift-resonant radial diffusion was derived assuming impulsive variations of the geomagnetic field and its induced electric field [*Kellogg*, 1959; *Parker*, 1960], which played a comparable role to ULF waves in the present work, and the pitch angle diffusion rate ($\mathcal{D}_{\alpha_0\alpha_0}$) was assumed longitudinally uniform due to theoretical tractability and the lack of in situ observations. *Roederer* [1968] [also *Schulz and Lanzerotti*, 1974, pp. 106 and 107] pointed out that under such a diffusion scheme, the energy-conserving anomalous radial diffusion provided extra acceleration for electrons diffusing into the radiation belts from an external source. Given that a typical electron PSD radial profile has a positive L gradient at fixed M and K and a negative gradient at fixed E, electrons have a favored inward diffusion at constant M and K and a favored outward diffusion at constant E. The consequence is that a fraction of the electrons would have repeated opportunities to gain energy by the energizing inward diffusion, and thus an enhanced PSD increase should occur.

Roederer's prediction seems contrary to the results in the current study. However, this apparent contradiction is caused by the different longitudinal distributions of pitch angle diffusion rate in the two schemes. In the picture of the phase space surfaces of Figure 7, with longitudinally uniform pitch angle diffusion rate, bounce-averaged diffusion in each Σ^* surface of a drift shell contributes equally to the drift-averaged diffusion, so that drift shell splitting causes much less systematic L shell dislocation of source regions due to cancellation from the oppositely curved dayside and nightside Σ^* surfaces. In contrast, in our diffusion scheme, the pitch angle scattering rate due to chorus waves is much greater in the nightside than the dayside, and Roederer's energization mechanism becomes secondary compared to the reduction of the source electron abundance. Since the chorus wave distribution is observationally derived, we would expect that a reduced PSD enhancement is more realistic.

As a practical consideration, for the radiation belt models that cannot deal with the $\langle D^*_{ML}\rangle$ and $\langle D^*_{KL}\rangle$ components, we have tested the effects of including $\langle D^*_{LL}\rangle$ alone as the drift shell splitting diffusion coefficient. In Figure 5, the PSD solutions obtained with only $\langle D^*_{LL}\rangle$ but not $\langle D^*_{ML}\rangle$ and $\langle D^*_{KL}\rangle$ (labeled ro for "radial only") are compared to those with the full set of drift shell splitting diffusion coefficients turned on or off. At POES factor 1, compared to off, the ro solution is even further separated from the on solution that incorporates the full set of starred diffusion components. This is expected since adding $\langle D^*_{LL}\rangle$ alone physically does not introduce any drift shell splitting but only increases radial diffusion at constant M and K. At larger peak POES factors, where chorus wave acceleration dominates the amount of PSD increase, the strengthened radial diffusion has very little effect on PSD.

In summary, we have shown, from simulations and theoretical arguments, that drift shell splitting decreases outer radiation belt electron PSD enhancements at small to intermediate K. This conclusion is derived from the basic geomagnetic field configuration that $\partial L/\partial\alpha_0 > 0$ in the nightside, the dominance of nightside over dayside chorus in resonant scattering, and the typically positive seed electron PSD radial gradient. Among these three premises, the first one is robust as it is a consequence of solar wind impinged on the geomagnetic field; the second one is statistically based and restricted to field-aligned chorus waves and might be unrealistic in a specific storm, especially with strong very oblique chorus waves; extreme magnetopause shadowing could render the last one invalid, in which case the conclusion of the current study is not applicable. The magnitude of the decrease depends on both the separation of the PSD source regions in L, which is determined by the asymmetry of the magnetic field, and the PSD radial gradient of the seed electrons. However, sensitivity of this decrease to each of the assumed premises is beyond the scope of this paper. In our simulations, we assumed a T89 magnetic field model with $Kp = 4$ and steady state radial diffusion in the initial and boundary conditions and found a nearly 1 order of magnitude decrease in PSD enhancement. In real magnetic storms where day-night magnetic field asymmetry could be more drastic, or electron injection events where the sustained source PSD radial gradient is much steeper, we would expect a stronger drift shell splitting effect than in our model. At last, we note that our study is confined in the realm of quasi-linear diffusion theory of radiation belts. Recent studies have brought into notice nonlinear wave acceleration of the electrons [e.g., *Mozer et al.*, 2014] and its potential modulation on seed electron profiles [e.g., *Ma et al.*, 2016]. Drift shell splitting effects under such energization mechanisms still remain an open question for future investigation.

Appendix A: Designing Initial and Boundary Conditions for the Radiation Belt Fokker-Planck Equation

In this appendix we seek, under certain assumptions and simplifying restrictions, an approximate special solution to the Fokker-Planck equation by separation of variables, for use in assigning initial and boundary conditions to equation (3).

For mathematical tractability, we consider bimodal radial and elastic pitch angle diffusion, which approximately conserves the quantity $\zeta \equiv M/y^2$ [*Walt*, 1970], where $y \equiv \sin\alpha_0$. In dipole field, the corresponding Fokker-Planck equation is [*Schulz and Lanzerotti*, 1974, p. 110]

$$\frac{\partial \bar{f}}{\partial t} = L^{\frac{5}{2}}\frac{\partial}{\partial L}\left[L^{-\frac{5}{2}}D_{LL}\frac{\partial \bar{f}}{\partial L}\right]_{x,\zeta} + \frac{1}{xT(y)}\frac{\partial}{\partial x}\left[xT(y)D_{xx}\frac{\partial \bar{f}}{\partial x}\right]_{\zeta,L}, \tag{A1}$$

where $x \equiv \cos\alpha_0$ and $T(y)$ is the normalized dipole bounce period. A special solution of (A1) can be obtained by assuming that the radial diffusion has reached a steady state, so that

$$L^{\frac{5}{2}}\frac{\partial}{\partial L}\left[L^{-\frac{5}{2}}D_{LL}\frac{\partial a}{\partial L}\right]_{x,\zeta} = 0, \tag{A2}$$

Equation (A1) becomes

$$\frac{\partial g}{\partial t} = \frac{1}{xT(y)}\frac{\partial}{\partial x}\left[xT(y)D_{xx}\frac{\partial g}{\partial x}\right]_{\zeta,L}, \tag{A3}$$

and $\bar{f}(t,\zeta,x,L)$ is given by

$$\bar{f}(t,\zeta,x,L) = a(\zeta,L)g(t,x) = a(\zeta,L)\sum_n g_n(x)\exp(-\lambda_n t), \tag{A4}$$

where $g_n(x)$ and λ_n are the eigenfunctions and eigenvalues of (A3). In a first-order approximation, for x-independent D_{xx} and constant loss cone cosine x_c, $g_n(x)$ is proportional to the zero order Bessel function $g_n(x) \propto J_0(\kappa_n x/x_c)$, where κ_n are roots of $J_0(\kappa_n) = 0$ [*Roberts*, 1969].

At fixed ζ, with the form $D_{LL} = D_0 L^\nu$ and the boundary conditions

$$\begin{cases} a(\zeta, L_1) = 0 \\ a(\zeta, L_2) = c'(\zeta) \end{cases} \qquad (1 < L_1 < L_2, \quad c'(\zeta) > 0), \tag{A5}$$

in which L_1 is the radial position of the radiation belt slot and L_2 an arbitrary outer position, the solution of (A2) is

$$\begin{aligned} a(\zeta, L) &= \frac{c'(\zeta)}{L_1^{\frac{7}{2}-\nu} - L_2^{\frac{7}{2}-\nu}} (L_1^{\frac{7}{2}-\nu} - L^{\frac{7}{2}-\nu}) \\ &\equiv c(\zeta) \left[1 - \left(\frac{L}{L_1} \right)^{\frac{7}{2}-\nu} \right], \qquad (L \geq L_1, \quad c(\zeta) > 0), \end{aligned} \tag{A6}$$

with $c(\zeta)$ a free function to be determined from the electron energy spectrum. Note that in integrating for (A6), we have tacitly assumed $\nu > 7/2$. For the purpose of designing a simple initial condition, we assume that at $t = 0$, $\bar{f}$ stays at the lowest eigenmode of pitch angle diffusion, which is arguably reasonable between storms [*O'Brien et al.*, 2014], so that

$$\bar{f}(0, \zeta, x, L) = c(\zeta) \left[1 - \left(\frac{L}{L_1} \right)^{\frac{7}{2}-\nu} \right] g_0(x). \tag{A7}$$

To find a simple form for $g_0(x)$, note that the lowest eigenfunction $J_0(\kappa_0 x/x_c)$ resembles the function $1-(x/x_c)^2$ [*Schulz and Lanzerotti*, 1974, pp. 162–166]. In the outer radiation belt, we may further assume that $x_c \simeq 1$ and hence use the simple form

$$g_0(x) \propto 1 - x^2. \tag{A8}$$

On the other hand, in dipole field particle momentum p is drift invariant, so we can phase average the particle flux j and obtain

$$\bar{j}(t, E, x, L) = p^2 \bar{f}(t, E, x, L) = \frac{2 m_0 \mu_E \zeta}{L^3 R_E^3} \bar{f}(t, E, x, L), \tag{A9}$$

where m_0 is the particle rest mass, μ_E is the Earth's dipole moment, and R_E is the Earth's radius. Assuming an exponential energy spectrum with e-folding energy E_0, the form of $\bar{j}$ is

$$\bar{j}(t, E, x, L) = \bar{j}(t, 0, x, L) \exp(-\frac{E}{E_0}), \tag{A10}$$

with kinetic energy

$$E = \mathcal{E}_0(\gamma - 1) = \mathcal{E}_0 \left(\sqrt{\frac{2\mu_E \zeta}{\mathcal{E}_0 R_E^3 L^3} + 1} - 1 \right), \tag{A11}$$

a function of ζ and L, where γ is the Lorentz factor and $\mathcal{E}_0$ is the rest energy.

Conservation of the first and second adiabatic invariants by radial diffusion implies that [*Schulz and Lanzerotti*, 1974, p. 131]

$$\left(\frac{\partial \ln \bar{j}}{\partial \ln p} \right)_{L,y} = \text{const.} \tag{A12}$$

For relativistic electrons, this restriction prescribes a relation for the e-folding energy that $E_0 L^{\frac{3}{2}} = \text{const}$, which is observationally evident (e.g., *Paolini et al.* [1968] report $E_0 L^{1.3} \simeq \text{const}$). With this relation, $\exp(-E/E_0)$ is only a weak function of L, and independent of L for highly relativistic electrons ($p^2c^2 \gg \mathcal{E}_0$). Combining (A7) through (A11), we have

$$\begin{aligned} \bar{f}(0, \zeta, x, L) &= c(\zeta) \left[1 - \left(\frac{L}{L_1} \right)^{\frac{7}{2}-\nu} \right] (1 - x^2) \\ &= \frac{R_E^3}{2 m_0 \mu_E} \frac{1}{\zeta} \exp\left(-\frac{E}{E_0} \right) L^3 \bar{j}(0, E = 0, x, L). \end{aligned} \tag{A13}$$

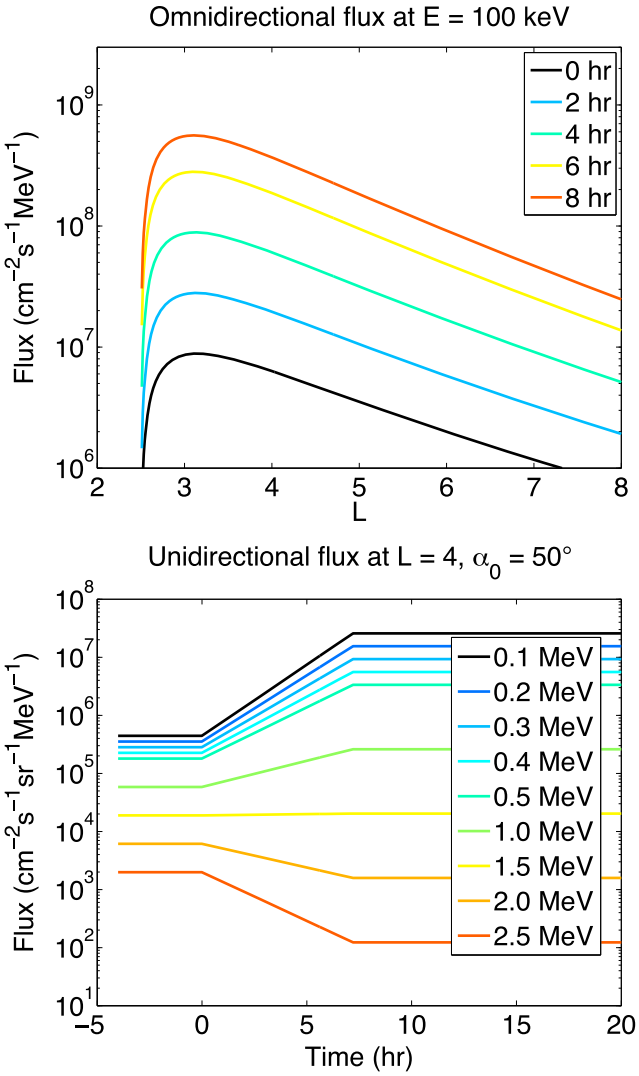

Figure A1. (top) Fitted omnidirectional electron fluxes on the low-energy boundary ($E = 100$ keV) versus L at different times and (bottom) fitted unidirectional fluxes at $L = 4$ and $\alpha_0 = 50°$ versus time for a range of electron energies. Here $t = 0$ corresponds to 02:30 UT 8 October 2012 (the onset of the low-energy electron injection). Figure A1 (bottom) shows that the low-energy electron injection is energy dependent, and high-energy (>1.5 MeV) electron fluxes decrease during the low-energy electron injection.

Therefore, comparison of variables between the two equations in (A13) yields

$$\bar{j}(0, E = 0, x, L) = \frac{\Gamma}{L^3}\left[1 - \left(\frac{L}{L_1}\right)^{\frac{7}{2}-\nu}\right](1 - x^2), \tag{A14}$$

which has a peak at $L = [(\nu - 1/2)/3]^{2/(2\nu-7)}L_1$, and

$$c(\zeta) \simeq \frac{R_E^3\Gamma}{2m_0\mu_E}\frac{1}{\zeta}\exp\left[-\frac{\mathcal{E}_0 L^{\frac{3}{2}}}{E_0'}\left(\sqrt{\frac{2\mu_E\zeta}{\mathcal{E}_0 R_E^3 L^3}} + 1 - 1\right)\right]. \tag{A15}$$

In these expressions, Γ is an arbitrary constant that scales the asymptotic "zero energy" equatorial flux amplitude

$$\bar{j}(0, E = 0, x = 0, L) = \frac{\Gamma}{L^3}, \qquad (L \gg L_1), \tag{A16}$$

and $E_0' = E_0 L^{\frac{3}{2}}$ a constant scaling the e-folding energy.

For Dirichlet boundary conditions, which must reduce to $\bar{f}(0,\zeta,x,L)$ on boundaries at $t=0$, $\bar{f}(t,\zeta,x,L)$ can be obtained by varying the two constants Γ and E_0' with time. Cast in more conventional variables, we have

$$\bar{f}(t,E,x,L)=\frac{\Gamma(t)}{L^3}\left[1-\left(\frac{L}{L_1}\right)^{\frac{7}{2}-\nu}\right]\frac{c^2}{E(E+2\mathcal{E}_0)}\exp\left[-\frac{EL^{\frac{3}{2}}}{E_0'(t)}\right](1-x^2), \tag{A17}$$

where c is the speed of light, and the values of $\Gamma(t)$ and $E_0'(t)$ are determined from fitting to observational data at different t. Note that comparing with (A4), we have absorbed the $\exp(-\lambda_0 t)$ term into $\Gamma(t)$. Exponential variations of the particle flux with time further restricts the functional forms of $\Gamma(t)$ and $E_0'(t)$. From equations (A10) to (A14), we have

$$\bar{j}(t,E,x=0,L)=\frac{\Gamma(t)}{L^3}\left[1-\left(\frac{L}{L_1}\right)^{\frac{7}{2}-\nu}\right]\exp\left[-\frac{E}{E_0'(t)}L^{\frac{3}{2}}\right], \tag{A18}$$

so that the time derivative

$$\frac{\partial}{\partial t}\ln\bar{j}(t,E,x=0,L)=\frac{1}{\Gamma}\frac{\mathrm{d}\Gamma}{\mathrm{d}t}-EL^{\frac{3}{2}}\frac{\mathrm{d}}{\mathrm{d}t}\left(\frac{1}{E_0'}\right) \tag{A19}$$

should be piecewise constant in t. Therefore, the functional forms of $\Gamma(t)$ and $E_0'(t)$ are

$$\Gamma(t)=\Gamma(0)\exp(\lambda t), \tag{A20}$$

$$\frac{1}{E_0'(t)}=\beta t+\frac{1}{E_0'(0)}, \tag{A21}$$

where λ and β are piecewise constant parameters to be determined from fitting to observational data. Figure A1 illustrates the fitted electron fluxes for the 8 October 2012 storm, as calculated from (A17) with $\nu=6$, corresponding to $Kp=4$ in the *Ozeke et al.* [2014] ULF wave diffusion coefficients, and the slot region position $L_1=2.5$.

The solution (A17) has the typical characteristics of a quiet time PSD: it has a positive L gradient at fixed M and K and a negative L gradient at fixed E and x beyond a peak. Thus, this initial condition can be understood as an approximation to the radiation belt after sufficient time of quiet magnetospheric conditions. On the low-energy boundary, equation (A17) physically assumes that the relaxation time for the seed electrons to radially diffuse to a steady state is much shorter than the characteristic time scale of the injection. On the Shabansky orbit boundary, where a 50 drift period (T_d) electron lifetime is assumed to schematically sketch the loss mechanism due to quasi-trapping, the boundary condition ($\bar{h}$) is multiplied by the factor as

$$\bar{h}(t,E,x,L)\Big|_{\text{boundary}}=\bar{f}(t,E,x,L)\exp\left(-\frac{t}{50T_d}\right)\Big|_{\text{boundary}}, \tag{A22}$$

in which T_d is also a function of E, x, and L.

Acknowledgments
This material is based upon work supported by the NASA Heliophysics Supporting Research (H-SR) Program under grant NNX15AI93G, the NASA Geospace Science Program under grant NNX10AL02G, the NASA Heliophysics Theory Program under grant NNX11AJ38G, NASA's Living With a Star Program through a Heliophysics Guest Investigator under grant NNX10AQ51G and through theory and modeling funding from the Van Allen Probes Mission's Energetic Particle, Composition, and Thermal Plasma (ECT) investigation, and by the U.S. Department of Energy through the LANL Laboratory Directed Research and Development (LDRD) Program. Van Allen Probes electron flux data used in this paper are taken from *Tu et al.* [2014]. The work by W. Tu was supported by NSF grant AGS-1613081 and NASA grant NNX15AW06G. We also acknowledge the PI and instrument team of the NOAA/POES SEM-2 instrument for providing data to the LANL coauthors. The drift shell splitting chorus wave diffusion coefficients can be obtained by contacting T.P. O'Brien at paul.obrien@aero.org.

References

Albert, J. M. (2009), The coupling of quasi-linear pitch angle and energy diffusion, *J. Atmos. Solar Terr. Phys.*, *71*(16), 1664–1668, doi:10.1016/j.jastp.2008.11.014.

Boyd, A. J., H. E. Spence, S. Claudepierre, J. F. Fennell, J. Blake, D. Baker, G. Reeves, and D. Turner (2014), Quantifying the radiation belt seed population in the 17 March 2013 electron acceleration event, *Geophys. Res. Lett.*, *41*, 2275–2281, doi:10.1002/2014GL059626.

Chen, Y., G. D. Reeves, R. H. W. Friedel, and G. S. Cunningham (2014), Global time-dependent chorus maps from low-Earth-orbit electron precipitation and Van Allen Probes data, *Geophys. Res. Lett.*, *41*, 755–761, doi:10.1002/2013GL059181.

Fälthammar, C.-G., and M. Walt (1969), Radial motion resulting from pitch-angle scattering of trapped electrons in the distorted geomagnetic field, *J. Geophys. Res.*, *74*(16), 4184–4186, doi:10.1029/JA074i016p04184.

Finlay, C. C., et al. (2010), International geomagnetic reference field: The eleventh generation, *Geophys. J. Int.*, *183*(3), 1216–1230, doi:10.1111/j.1365-246x.2010.04804.x.

Kellogg, P. J. (1959), Van Allen radiation of solar origin, *Nature*, *183*, 1295–1297, doi:10.1038/1831295a0.

Kim, H.-J., E. Zesta, K.-C. Kim, Y. Shprits, Y. Shi, and L. R. Lyons (2010), Estimation of radial gradients of phase space density from POLAR observations during a quiet period prior to a sudden solar wind dynamic pressure enhancement, *J. Geophys. Res.*, *115*, A12249, doi:10.1029/2010JA015722.

Li, W., Y. Y. Shprits, and R. M. Thorne (2007), Dynamic evolution of energetic outer zone electrons due to wave-particle interactions during storms, *J. Geophys. Res.*, *112*, A10220, doi:10.1029/2007JA012368.

Li, W., B. Ni, R. M. Thorne, J. Bortnik, J. C. Green, C. A. Kletzing, W. S. Kurth, and G. B. Hospodarsky (2013), Constructing the global distribution of chorus wave intensity using measurements of electrons by the POES satellites and waves by the Van Allen Probes, *Geophys. Res. Lett.*, *40*, 4526–4532, doi:10.1002/grl.50920.

Liu, S., et al. (2015), Van Allen Probes observations linking radiation belt electrons to chorus waves during 2014 multiple storms, *J. Geophys. Res. Space Physics*, *120*, 938–948, doi:10.1002/2014JA020781.
Ma, Q., D. Mourenas, A. Artemyev, W. Li, R. M. Thorne, and J. Bortnik (2016), Strong enhancement of 10–100 keV electron fluxes by combined effects of chorus waves and time domain structures, *Geophys. Res. Lett.*, *43*, 4683–4690, doi:10.1002/2016GL069125.
Mozer, F. S., O. Agapitov, V. Krasnoselskikh, S. Lejosne, G. D. Reeves, and I. Roth (2014), Direct observation of radiation-belt electron acceleration from electron-volt energies to megavolts by nonlinear whistlers, *Phys. Rev. Lett.*, *113*, 35001, doi:10.1103/PhysRevLett.113.035001.
Norman, C. W. (1986), *Undergraduate Algebra*, Oxford Univ. Press, New York.
O'Brien, T. P. (2014), Breaking all the invariants: Anomalous electron radiation belt diffusion by pitch angle scattering in the presence of split magnetic drift shells, *Geophys. Res. Lett.*, *41*, 216–222, doi:10.1002/2013GL058712.
O'Brien, T. P. (2015), The activity and radial dependence of anomalous diffusion by pitch angle scattering on split magnetic drift shells, *J. Geophys. Res. Space Physics*, *120*, 328–343, doi:10.1002/2014JA020422.
O'Brien, T. P., S. G. Claudepierre, J. B. Blake, J. F. Fennell, J. H. Clemmons, J. L. Roeder, H. E. Spence, G. D. Reeves, and D. N. Baker (2014), An empirically observed pitch-angle diffusion eigenmode in the Earth's electron belt near $L^* = 5.0$, *Geophys. Res. Lett.*, *41*, 251–258, doi:10.1002/2013GL058713.
Onsager, T. G., A. A. Chan, Y. Fei, S. R. Elkington, J. C. Green, and H. J. Singer (2004), The radial gradient of relativistic electron phase-space density at geosynchronous orbit, *J. Geophys. Res.*, *109*, A05221, doi:10.1029/2003JA010368.
Ozeke, L. G., I. R. Mann, K. R. Murphy, I. Jonathan Rae, and D. K. Milling (2014), Analytic expressions for ULF wave radiation belt radial diffusion coefficients, *J. Geophys. Res. Space Physics*, *119*, 1587–1605, doi:10.1002/2013JA019204.
Öztürk, M. K., and R. A. Wolf (2007), Bifurcation of drift shells near the dayside magnetopause, *J. Geophys. Res.*, *112*, A07207, doi:10.1029/2006JA012102.
Paolini, F., G. Theodoridis, S. Frankenthal, and L. Katz (1968), Radial diffusion processes of relativistic outer-belt electrons, *Ann. Geophys.*, *24*, 129–135.
Parker, E. N. (1960), Geomagnetic fluctuations and the form of the outer zone of the Van Allen radiation belt, *J. Geophys. Res.*, *65*(10), 3117–3130, doi:10.1029/JZ065i010p03117.
Roberts, C. S. (1969), Pitch-angle diffusion of electrons in the magnetosphere, *Rev. Geophys.*, *7*(1-2), 305–337, doi:10.1029/RG007i001p00305.
Roederer, J. G. (1967), On the adiabatic motion of energetic particles in a model magnetosphere, *J. Geophys. Res.*, *72*(3), 981–992, doi:10.1029/JZ072i003p00981.
Roederer, J. G. (1968), Shell splitting and radial diffusion of geomagnetically trapped particles, in *Earth's Particles and Fields*, vol. 1, edited by B. M. McCormac, p. 193, Reinhold Publ. Corp., New York.
Roederer, J. G. (1970), *Dynamics of Geomagnetically Trapped Radiation, Physics and Chemistry in Space*, vol. 2, Springer-Verlag, New York.
Roederer, J. G., and M. Schulz (1969), Effect of shell splitting on radial diffusion in the magnetosphere, *J. Geophys. Res.*, *74*(16), 4117–4122, doi:10.1029/JA074i016p04117.
Santolík, O., J. S. Pickett, D. A. Gurnett, J. D. Menietti, B. T. Tsurutani, and O. Verkhoglyadova (2010), Survey of Poynting flux of whistler mode chorus in the outer zone, *J. Geophys. Res.*, *115*, A00F13, doi:10.1029/2009JA014925.
Schulz, M. (1972), Drift-shell splitting at arbitrary pitch angle, *J. Geophys. Res.*, *77*(4), 624–634, doi:10.1029/JA077i004p00624.
Schulz, M. (1996), Canonical coordinates for radiation-belt modeling, in *Radiation Belts: Models and Standards*, edited by J. F. Lemaire, D. Heynderickx, and D. N. Baker, pp. 153–160, AGU, Washington, D. C.
Schulz, M., and L. J. Lanzerotti (1974), *Particle Diffusion in the Radiation Belts*, Springer, New York.
Shabansky, V. P. (1971), Some processes in the magnetosphere, *Space Sci. Rev.*, *12*, 299–418.
Sheeley, B. W., M. B. Moldwin, H. K. Rassoul, and R. R. Anderson (2001), An empirical plasmasphere and trough density model: CRRES observations, *J. Geophys. Res.*, *106*(A11), 25,631–25,641, doi:10.1029/2000JA000286.
Shprits, Y., D. Subbotin, B. Ni, R. Horne, D. Baker, and P. Cruce (2011), Profound change of the near-Earth radiation environment caused by solar superstorms, *Space Weather*, *9*, S08007, doi:10.1029/2011SW000662.
Shprits, Y. Y., and B. Ni (2009), Dependence of the quasi-linear scattering rates on the wave normal distribution of chorus waves, *J. Geophys. Res.*, *114*, A11205, doi:10.1029/2009JA014223.
Tao, X., A. A. Chan, J. M. Albert, and J. A. Miller (2008), Stochastic modeling of multidimensional diffusion in the radiation belts, *J. Geophys. Res.*, *113*, A07212, doi:10.1029/2007JA012985.
Thorne, R. M., B. Ni, X. Tao, R. B. Horne, and N. P. Meredith (2010), Scattering by chorus waves as the dominant cause of diffuse auroral precipitation, *Nature*, *467*(7318), 943–946.
Tsyganenko, N. (1989), A magnetospheric magnetic field model with a warped tail current sheet, *Planet. Space Sci.*, *37*(1), 5–20, doi:10.1016/0032-0633(89)90066-4.
Tu, W., G. S. Cunningham, Y. Chen, S. K. Morley, G. D. Reeves, J. B. Blake, D. N. Baker, and H. Spence (2014), Event-specific chorus wave and electron seed population models in DREAM3D using the Van Allen Probes, *Geophys. Res. Lett.*, *41*, 1359–1366, doi:10.1002/2013GL058819.
Ukhorskiy, A. Y., M. I. Sitnov, R. M. Millan, and B. T. Kress (2011), The role of drift orbit bifurcations in energization and loss of electrons in the outer radiation belt, *J. Geophys. Res.*, *116*, A09208, doi:10.1029/2011JA016623.
Walt, M. (1970), Radial diffusion of trapped particles, in *Particles and Fields in the Magnetosphere*, edited by B. M. McCormac, pp. 410–415, Springer, New York.
Zheng, L. (2015), Development and application of stochastic methods for radiation belt simulations, PhD thesis, Rice University, Houston, Tex.
Zheng, L., A. A. Chan, J. M. Albert, S. R. Elkington, J. Koller, R. B. Horne, S. A. Glauert, and N. P. Meredith (2014), Three-dimensional stochastic modeling of radiation belts in adiabatic invariant coordinates, *J. Geophys. Res. Space Physics*, *119*, 7615–7635, doi:10.1002/2014JA020127.
Zorich, V. A. (2004), *Mathematical Analysis*, vol. 2, Springer, Berlin, English edition translated by R. Cooke.